Development of DPD coarse-grained models: From bulk to interfacial properties

José G. Solano Canchaya,[1,2] Alain Dequidt,[1,2,a)] Florent Goujon,[1,2] and Patrice Malfreyt[1,2]
[1]*Institut de Chimie de Clermont-Ferrand, Université Blaise Pascal, Université Clermont Auvergne, BP 10448, F-63000 Clermont-Ferrand, France*
[2]*CNRS, UMR 6296, ICCF, F-63178 Aubiere, France*

(Received 20 May 2016; accepted 19 July 2016; published online 2 August 2016)

A new Bayesian method was recently introduced for developing coarse-grain (CG) force fields for molecular dynamics. The CG models designed for dissipative particle dynamics (DPD) are optimized based on trajectory matching. Here we extend this method to improve transferability across thermodynamic conditions. We demonstrate the capability of the method by developing a CG model of *n*-pentane from constant-NPT atomistic simulations of bulk liquid phases and we apply the CG-DPD model to the calculation of the surface tension of the liquid-vapor interface over a large range of temperatures. The coexisting densities, vapor pressures, and surface tensions calculated with different CG and atomistic models are compared to experiments. Depending on the database used for the development of the potentials, it is possible to build a CG model which performs very well in the reproduction of the surface tension on the orthobaric curve. *Published by AIP Publishing.* [http://dx.doi.org/10.1063/1.4960114]

I. INTRODUCTION

The development of coarse-grained (CG) models for modeling biomolecular processes and polymeric materials at larger lengths and time scales[1–4] is an area of active research. Coarse-graining of a molecule consists of reducing the number of degrees of freedom and averaging the molecule into a number of CG particles often called "beads." This simplified representation of the structure and of the underlying interactions allows for longer lengths and time scales than atomistic models.[5–7] However, the choice of degrees of freedom to be averaged into a bead may impact significantly the simulated properties.[4,8] The key-problem is how to simplify the model while preserving the essential physical behaviour specific to the chemical nature of the molecule. The reader is directed to a number of discussions of the advantages and drawbacks of the CG models.[9–13]

As a result, the challenge consists in building realistic CG force fields. There are two approaches to designing CG models. The top-down approach derives the parameters from macroscopic experimental data.[14–16] The bottom-up uses a multiscale model based on atomic simulations.[17–21] Useful bottom-up CG strategies include the iterative Boltzmann inversion (IBI)[22,23] and force matching (FM)[17,24] schemes. It is clear that the success of the CG force field will depend on the transferability of its parameters. This is an open issue since the transferability must be discussed at different levels: the transferability of the chemical groups to different molecules and the transferability to different thermodynamic conditions (temperature and pressure). It results that the performance of the CG model must be validated through different simulation conditions (temperature, pressure, composition, timestep, bulk phases, interfaces, . . .).

Different CG force fields[5,16,25–27] use different mappings or degrees of coarse-graining. This level of coarse-graining ranges from 4:1 (a CG particle represents four heavy atoms plus associated hydrogen atoms)[25] to 20:1 (one CG particle corresponds to 20 united atoms).[5–7] Some models such as the MARTINI force field[25,26] developed by Marrink, de Vries, and Mark model the dispersion and overlap interactions with a 12-6 shifted Lennard-Jones (LJ) potential, while Klein and co-workers[28] prefer a 9-6 LJ potential, and Chiu, Scott, and Jakobsson[27] have employed a Morse potential to study alkanes and water. The MARTINI model has been developed from the calculation of the free energy of hydration, the free energy of vaporization, and the partitioning free energies between water and a number of organic phases. Again, Avendaño *et al.*[16] have developed the (SAFT-γ) CG force field from the Statistical Associating Fluid Theory (SAFT) equation of state,[29,30] using the Mie-generalized Lennard-Jones potential. All these force fields have been used with standard Monte Carlo (MC) and molecular dynamics (MD) methods.

The use of CG models for the modeling of interfacial systems and the calculation of the interfacial tension is much less widespread due to the fact that these CG models have never been adjusted on this interfacial property. However, these CG models represent a challenging approach to investigate the temperature and pressure dependences of the interfacial tension of complex micellar systems. Actually, the simulation of oil-surfactant-water mixtures needs large system-sizes and also a very long simulation since the equilibration of the surfactant between the bulk and interface regions is slow. Before tackling such problems and giving a quantitative answer to the calculation of the interfacial tension, some CG models have been tested on simpler interfaces. The

a)Electronic mail: alain.dequidt@univ-bpclermont.fr

Reuse of AIP Publishing content is subject to the terms: https://publishing.aip.org/authors/rights-and-permissions. Downloaded to IP: 195.221.123.85 On: Wed, 17 Aug 2016 07:32:51

MARTINI model performs better in the case of the liquid-vapor (LV) interface of alkanes.[26] This type of molecules is the best candidate for a coarse-grained approach since it is formed by a number of identical groups that interact predominantly through dispersion-repulsion interactions. Another coarse-graining strategy, based on the models of Mie segments, has been successfully applied to calculate the surface tension of liquid-vapor interfaces[16,31] of CO_2, SF, CH_4, and long linear alkanes including n-$C_{10}H_{22}$ and n-$C_{20}H_{42}$. For linear alkanes, CG models based on the 12-6 Lennard-Jones potential for the calculation of the nonbonded interactions have been developed to reproduce successfully the coexisting densities and surface tensions at different temperatures.[32] For water, the situation is different. Actually, the first simulations of the liquid-vapor interface of water with the MARTINI CG force field[26] gave values of surface tensions of 45 mN m^{-1} at 298 K. For the polarizable version of the water MARTINI model,[33] the simulated surface tension is 30 mN m^{-1}. This significant deviation from experiments (γ_{exp} = 73 mN m^{-1}) can be explained by the absence of significant ordering of the dipoles of the CG water particles in the interfacial region.[33] Recently, we have used the MARTINI force field for the calculation of the interfacial tension of various liquid-liquid interfaces.[8] We concluded that the interfacial tension could be reproduced within ±10 mN m^{-1} with respect to experiments.

Other CG potentials can be used with mesoscopic methods such as dissipative particle dynamics (DPD).[34–37] Dissipative particle dynamics[34,35,37,38] (DPD) is an interesting option for CG models, typically allowing for longer time steps than atomistic simulations. The term DPD is often associated with a quadratic soft conservative potential model,[35] but different shapes of potential models have been used with this mesoscopic method.[6,7,39] The Green-Kubo approach for parameterizing DPD models from bottom-up applies in principle when there is a clear separation of the timescale between the degrees of freedom of the CG model and the other atomistic degrees of freedom which are discarded in the CG model.[21,40,41] However, the contribution of the missing degrees of freedom in any CG model can be modeled using dissipative and random forces as in DPD. These forces should in theory only impact the dynamic properties of the CG system. As regards to static properties the results obtained with a DPD model at equilibrium should be the same as those of a non-dissipative CG model using the same conservative interactions. Most of the CG models used for simulating liquid-vapor interfaces are either non-dissipative[14,32] or use density-dependent manybody interactions.[36,37,42,43]

Concerning the calculation of interfacial tensions from mesoscopic DPD simulations using soft multi-body potentials, we have reported a good reproduction of the surface tension of the liquid-vapor (LV) interface of water in a relatively small range of temperature from 275 K to 325 K.[37] The parameters of the multi-body potential have been developed from a top-down approach.[37] This MDPD method has also been extended to the case of the liquid-vapor interface of mixtures[43] and electrolytes.[44,45] Standard DPD simulations have also been used to calculate the interfacial tensions of liquid-liquid interfaces[43,46,47] where the parameters of the conservative potentials have been developed from the Flory-Huggins parameter by means of the solubility parameters.[47]

One may question whether the CG DPD models designed following the bottom-up approach from atomistic configurations of bulk phases can be applied to produce quantitative liquid-vapor interfacial tensions. In the present article, we develop and characterize a CG DPD model using a Bayesian optimization procedure recently introduced (see Ref. 39). This method was used to build a DPD model of pentane at 300 K, with static and dynamic properties close to the atomistic simulations used as a reference. We propose to show that the CG potential developed from bulk atomistic simulations in the constant-*NPT* ensemble is reasonably transferable in temperature and pressure for different thermodynamic properties such as surface tension, coexisting densities, and vapor pressures. To our knowledge, this is the first DPD model reproducing LV equilibria without considering any manybody interactions.[37] An improved version of the CG DPD model, regarding transferability and critical point, will be proposed using a multi-temperature set of reference atomistic simulations. The DPD model parameters yet remain temperature-independent.

The paper is organized as follows: In Section II, we describe the theoretical background of the method used for parameterizing the CG model of pentane. In Section III, we explain how the CG potential was obtained and study the transferability of the static properties in the case of bulk DPD systems. In Section IV, we focus on the properties of the DPD LV interfaces. We conclude in Section V by a summary of our main results.

II. BAYESIAN OPTIMIZATION OF THE COARSE-GRAIN MODEL

The coarse-grain DPD potentials were constructed using the method recently described in Ref. 39. This is a kind of force matching method, which takes into account the dissipative and random forces of the DPD model. As an input, a reference trajectory is required. The trajectory denoted by $\mathcal{T}$ consists of the set of successive positions of the CG degrees of freedom. It can be obtained by running a high resolution atomistic simulation of the molecular dynamics and deducing the coordinates of the CG degrees of freedom from the atomic positions. The optimization procedure determines the parameters of the CG model, which are the most likely to produce the reference trajectory. It allows for determining at the same time the conservative and dissipative parameters.

Knowing the successive coordinates R_t^{ref} of the CG degrees of freedom, their velocities V_t^{ref} and accelerations or forces F_t^{ref} can be deduced. As shown in Ref. 39 by assuming a Gaussian distribution of random forces, the optimization is equivalent to minimizing

$$\mathcal{L}(x) = \frac{1}{2}\sum_{t\in\mathcal{T}} \log \det{}_{+}\Gamma_t + \frac{\Delta t\, F_t^{R*}\Gamma_t^{+}F_t^{R}}{2\,k_BT}. \qquad (1)$$

In this equation, x is the set of parameters of the CG model to be optimized, Δt is the CG timestep, i.e., the time between successive configurations in the reference trajectory, and k_BT

Reuse of AIP Publishing content is subject to the terms: https://publishing.aip.org/authors/rights-and-permissions. Downloaded to IP: 195.221.123.85 On: Wed, 17 Aug 2016 07:32:51

is the thermal energy. F_t^R is the random contribution to the vector of total forces felt by the CG degrees of freedom at time t. The following can be deduced from the reference forces, knowing the conservative $F_t^C = F^C(R_t^{\text{ref}}, x)$ and dissipative forces $F_t^D = -\Gamma_t V_t^{\text{ref}}$:

$$F_t^R = F_t^{\text{ref}} - F_t^C - F_t^D. \tag{2}$$

$\Gamma_t = \Gamma(R_t^{\text{ref}})$ is the global symmetric positive friction matrix at time t, such that

$$\left\langle F_t^R \, F_{t'}^{R*} \right\rangle = 2\,\Gamma_t \, k_B T \, \delta(t - t'). \tag{3}$$

Superscript * denotes matrix transposition while superscript $^+$ denotes Moore-Penrose pseudoinverse. Indeed, Γ_t is structurally singular when the system conserves total momentum, so that Γ^+ has to be used instead of Γ^{-1}. For the same reason, the pseudodeterminant $\det^+$, which is the product of all non-zero eigenvalues, has to be used instead of the standard determinant.

It was already noted in Ref. 39 that volume can be included in the set of CG degrees of freedom if the reference trajectory was obtained in the constant-*NPT* ensemble using periodic boundary conditions. In particular, this allows for developing a CG model which reproduces the reference density.

When the model defines conservative interactions as a linear combination of the CG parameters, an analytical optimum can be found. In this case,

$$F_t^C = A_t \, x \tag{4}$$

with $A_t = A(R_t^{\text{ref}})$ a matrix; the optimal x is given by

$$\bar{x} = \left(\sum_t A_t^* \, \Gamma_t^+ \, A_t \right)^+ \left(\sum_t A_t^* \, \Gamma_t^+ \, F_t^{\text{ref}} \right). \tag{5}$$

For developing a multi-temperature CG potential, reference trajectories at different temperatures can be used. The generalization is straightforward and yields the optimal x as

$$\bar{x}^{MT} = \left(\sum_{\mathcal{T}} \frac{1}{T_{\mathcal{T}}} \sum_{t \in \mathcal{T}} A_t^* \, \Gamma_t^+ \, A_t \right)^+ \left(\sum_{\mathcal{T}} \frac{1}{T_{\mathcal{T}}} \sum_{t \in \mathcal{T}} A_t^* \, \Gamma_t^+ \, F_t^{\text{ref}} \right), \tag{6}$$

where $T_{\mathcal{T}}$ is the temperature of trajectory $\mathcal{T}$.

In the present article we are only interested in static properties, so that we should only focus on the conservative parameters of the model. Nevertheless, for completeness we also give the expression of the optimal dissipative parameter. The dissipative matrix Γ_t can be built from pairwise dissipative interactions in the form given by Español and Warren[38] with a single unknown parameter γ, the amplitude of the friction. The dissipative force exerted by i on j is

$$f_{ij}^D = -\gamma \left(1 - \frac{|r_{ij}|}{r_d} \right)^2 (v_j - v_i)_{\parallel}, \quad |r_{ij}| < r_d, \tag{7}$$

where $\parallel$ means projected along the r_{ij} vector and r_d is a cutoff beyond which $f_{ij}^D = 0$. So the friction matrix can be expressed as $\Gamma_t = \gamma \, B_t$, with B_t a matrix independent of γ. With this expression of the dissipative forces, the optimal friction parameter $\bar{\gamma}$ can be found by solving $\frac{\partial \mathcal{L}}{\partial \gamma} = 0$. For multi-temperature reference trajectories one gets

$$0 = \bar{\gamma}_{MT} \frac{2\,N\,k_B}{\Delta t} + \bar{\gamma}_{MT}^2 \frac{1}{n_t} \sum_{\mathcal{T}} \frac{1}{T_{\mathcal{T}}} \sum_{t \in \mathcal{T}} V_t^* B_t V_t - \frac{1}{n_t} \sum_{\mathcal{T}} \frac{1}{T_{\mathcal{T}}} \sum_{t \in \mathcal{T}} (F_t^{\text{ref}} - F_t^C)^* B_t^+ (F_t^{\text{ref}} - F_t^C) \tag{8}$$

with $N = 3n - 2$ the number of independent degrees of freedom and $n_t = \sum_{\mathcal{T}} \sum_{t \in \mathcal{T}} 1$ the number of configurations for which F_t^{ref} can be computed.

III. PARAMETERIZATION OF THE CG MODEL FROM BULK REFERENCE SIMULATIONS

For testing our methodology we have chosen a liquid *n*-pentane system. For the purpose of this work, MD simulations at different temperatures were carried out using the DL_POLY code[48] in order to create the reference atomic trajectories. As initial sample we used a cubic simulation box comprising 700 *n*-pentane molecules with a box side length of $L \sim 50$ Å under periodic boundary conditions where the *n*-pentane molecules are modeled using the TraPPE force field.[49] Analytical expressions and parameters describing the potential can be found in Refs. 49–51.

A series of MD simulations with 12 different temperatures in the ascending order, T = 200, 250, 300, 350, 400, 410, 420, 430, 440, 450, 460, and 470 K, are sequentially performed in the constant-*NPT* ensemble at $P = 0.1$ MPa using the Berendsen[52] barostat algorithm. The first MD simulation is carried out at $T = 200$ K for 2 ns where the statistical information is collected during the last 1 ns. The following MD simulation at the next higher temperature is performed starting from the configuration obtained in the previous MD simulation at lower temperature. For all these simulations the system was initially equilibrated for 500 ps followed by a production run of 1 ns. In all cases we use a timestep of $\delta t = 2$ fs. During the production stage positions of all the particles together with the unit cell volume were recorded every 25 timesteps. As a result we obtained a reference atomistic trajectory comprising 20 000 configurations for each temperature that can be used for the subsequent CG-modelling. It is important to mention that in order to get a reference system in a liquid phase for temperatures above $T = 430$ K the simulations were carried out at the critical pressure of *n*-pentane $P_c = 3360$ kPa.

For all the obtained trajectories each *n*-pentane molecule was coarse-grained into a single bead, where positions of the beads coincide with the center of mass (COM) of the atoms corresponding to each bead. The degree of coarse-graining was 5:1. This coarse-graining procedure was repeatedly performed onto successive saved configurations for each recorded MD trajectory in order to create the CG trajectory $\mathcal{T}(\bar{R}_t^{\text{CG}})$ with a time interval value $\Delta t = 50$ fs. The bead velocities $\bar{V}_t^{\text{ref}}$ and the total forces $\bar{F}_t^{\text{ref}}$ acting on each bead were derived using the expressions provided in our previous work.[39]

The conservative force F_t^C between beads is described by a linear combination of triangular basis functions resulting in a set $\{x_i^C\}$ of unknown parameters. This corresponds to a tabulated interaction force with linear interpolation. We have used a total of 20 basis functions and a cutoff radius

Reuse of AIP Publishing content is subject to the terms: https://publishing.aip.org/authors/rights-and-permissions. Downloaded to IP: 195.221.123.85 On: Wed, 17 Aug 2016 07:32:51

of r_C = 20 Å, and thus the tabulated values are equidistantly spaced with a mesh size of 1 Å. For the dissipative and random forces F^D and F^R we have used the analytical expression of Eq. (7) with a value of r_d = 20 Å. Further details can be found in our previous paper.[39]

The optimal parameters $\{\bar{x}_i^{MT}\}$ were determined by numerically solving the expression given in Eq. (6). The optimal value for the friction coefficient $\bar{\gamma}^{MT}$ was then evaluated by solving directly Eq. (8) once the optimal $\{\bar{x}_i^{MT}\}$ are found. In Figure 1 the resulting multi-temperature conservative potential U_{MT}^C is represented along with the single-temperature potentials. U_T^C was calculated by solving the expression given in Eq. (5) for each independent $\mathcal{T}_T$. It can be seen that in all cases the potential presents a strongly repulsive part and a weakly attractive part. The position of the minimum moves from 10 Å at low temperatures to 7 Å at higher temperatures. The multi-temperature potential is closer to the high temperature potentials.

To establish the validity of our method, DPD simulations were carried out using the optimal set $\{\bar{x}_i^{MT}\}$ and $\bar{\gamma}^{MT}$ = 15.65 kg mol^{-1} ns^{-1} in a simulation box containing 700 beads. The initial configuration and box size were taken from the last recorded frame of the CG trajectory corresponding to the lowest temperature of MD simulations. The DPD simulations were performed at different temperatures at a pressure P = 0.1 MPa using the same annealing procedure used for MD calculations.

For comparison with the iterative Boltzmann inversion method[22,23] we computed the radial distribution function (RDF) between CG sites using the reference trajectories saved from the MD simulations and from DPD simulations using the multi-temperature potential U_{MT}^C. A comparison of the RDFs at different temperatures is shown in Figure 2. It is seen that our approach produces consistent agreement between RDFs. Indeed, the main characteristics of the coarse-grained MD RDFs are reproduced by our DPD model. We emphasize that this agreement was obtained although the optimization process is not based on fitting RDFs as with iterative Boltzmann inversion. Let us also remind that the agreement between RDFs, though desirable, is not the key factor for predicting accurately the bulk and interfacial properties.[53]

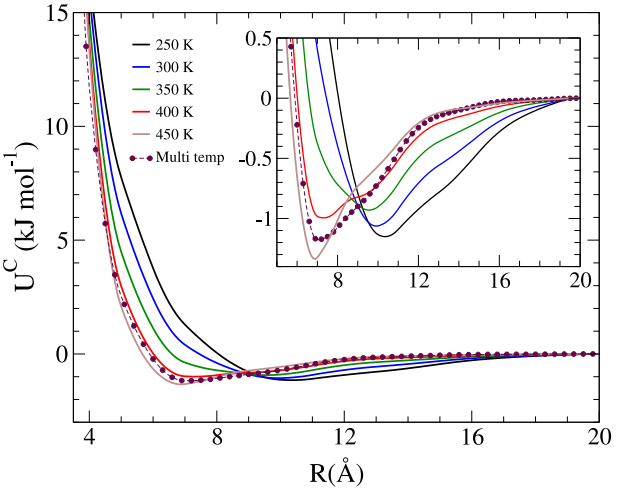

FIG. 1. Pairwise conservative potential U^C versus the intermolecular distance R obtained for n-pentane at T = 250, 300, 350, 400, and 450 K. (•) represent the multi-temperature CG potential. The constant-NPT simulations were performed with r_C = 20 Å, r_D = 20 Å.

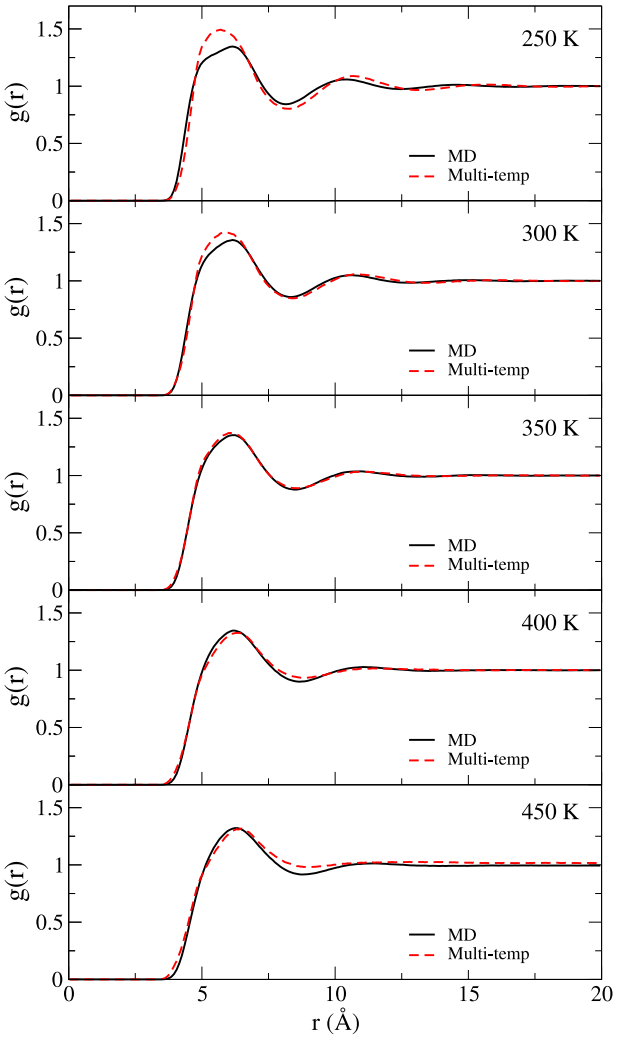

FIG. 2. Radial distribution function for liquid n-pentane obtained at various temperatures and P = 0.1 MPa (3.36 MPa at 450 K) from coarse-grained MD trajectories and compared to those obtained from DPD dynamics using the multi-temperature potential U_{MT}^C.

More quantitatively, it is noticeable that at lower temperatures the first peak of the DPD-RDF is higher and that a slight right shift of the peak maximum appears. The corresponding excess of neighbors in the first shell is quantified in Table I. It can be related to the slight excess of density which appears at low temperature (Figure 3).

TABLE I. Average number of neighbours in the first shell at different temperatures in the MD simulations and in the DPD simulations using the multi-temperature potential U_{MT}^C.

T (K)	MD	DPD	Relative deviation (%)
250	11.58	12.97	+12
300	11.51	12.14	+5
350	11.29	11.51	+2
400	10.21	10.78	+6
450	8.82	10.10	+14

Reuse of AIP Publishing content is subject to the terms: https://publishing.aip.org/authors/rights-and-permissions. Downloaded to IP: 195.221.123.85 On: Wed, 17 Aug 2016 07:32:51

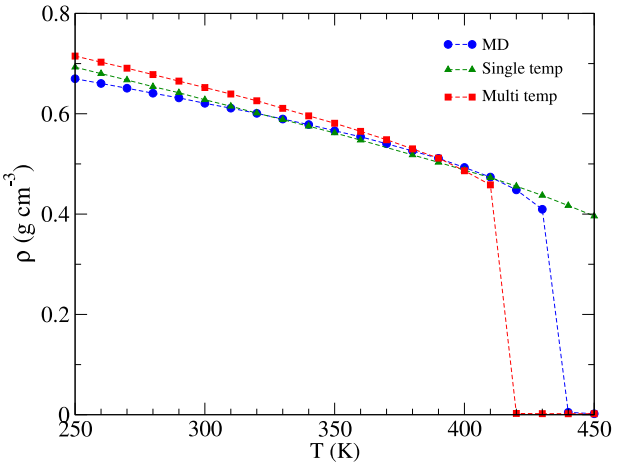

FIG. 3. Calculated densities at $P = 1$ atm for liquid *n*-pentane from the atomistic MD simulations and from CG DPD simulations using the multi-temperature potential U_{MT}^{C} and a single temperature potential U_{T}^{C} with $T = 300$ K.

The densities calculated in the constant-*NPT* ensemble of the liquid *n*-pentane ranging from 250 to 450 K under constant (1 atm) pressure are shown in Figure 3. Note that the bulk systems under *NPT* conditions at high temperatures are in metastable states, as it will be seen in the vapor pressure analysis (Section IV). It is also observed that the multi-temperature CG model reproduces very well the MD densities. The liquid-vapor transition temperature (spinodal curve) is lower than the MD reference. For comparison the single temperature CG model (T = 300 K) has a very high spinodal temperature compared to the other models.

At this point we have established that the optimized DPD models are able to satisfactorily reproduce the static properties (structure and density) of the bulk phase. We stress that it is crucial to use the constant-*NPT* ensemble for the MD trajectories to obtain the agreement on density. The use of *NVT* reference trajectories that consist in not considering the volume dynamics yields a much less attractive DPD potential, and the DPD equilibrium density at constant pressure is poorly reproduced. This is exactly what we observed when reproducing the density of polymer chains for which only the bottom-up approach developed in the constant-*NPT* ensemble performs in the reproduction of this property.[5,6] In Sec. IV we study the interfacial properties that are obtained using the DPD potential optimized with bulk liquid phases.

IV. INTERFACIAL PROPERTIES OF THE CG MODEL

DPD simulations in the constant-*NVT* ensemble were carried out to study the liquid-vapor equilibrium properties of *n*-pentane. The simulations were performed within a rectangular parallelipipedic simulation box of dimensions $L_x = L_y = 4.1$ nm, $L_z = 100$ nm containing 3500 single bead pentane molecules. Doing so, L_x and L_y are slightly above twice the interaction cutoff. The periodic boundary conditions are applied in the three directions. The initial configuration has been built by placing the pentane beads inside a slab in the middle of the box with a density corresponding to bulk liquid pentane. An initial constant-*NVT* simulation was performed for over 2 ns in order to obtain an equilibrated configuration to use as the starting point. Then, the temperature of the system was increased from 200 K to 500 K by steps of 10 K. At each temperature, the system was first equilibrated for 500 ps followed by an acquisition phase of 2 ns where statistical information was collected. The final configuration was then used as the starting configuration for the next higher temperature. This procedure was repeated up to the highest temperature. In all simulations, the integration time step was Δt = 50 fs and the statistical data were collected every 100 steps except for the density and pressure profiles for which data were accumulated every step. In order to create reference data to compare the performance of our DPD model MD simulations were also performed for a liquid-vapor system. For MD simulations we have used a similar but smaller simulation box of dimensions $L_x = L_y = 2.5$ nm, $L_z = 10$ nm containing 700 *n*-pentane molecules. A similar annealing process as in DPD simulations was used for our MD simulations with an integration timestep of $\delta t = 2$ fs, an equilibration time of 400 ps, and a acquisition time of 2 ns.

The density profiles were calculated in the direction normal to the interface, $\rho(z)$, by splitting the cell into slabs of width Δz. In Figure 4 the density profiles calculated from DPD simulations are shown for four temperatures. First, the DPD CG model reproduces successfully the liquid-vapor coexistence by showing two well-developed liquid and vapor regions. Let us notice that the DPD CG models developed in the constant-*NVT* ensemble are unable to lead to a liquid-vapor equilibrium owing to a less deep attractive part of the CG potential. The profiles are symmetrical with respect to the center of the box indicating well-converged slab simulations. The liquid phase roughly extends over 40 Å. The changes in the profiles with the temperatures are in line with those expected by the thermodynamics. For increasing temperatures, we observe a decrease of the liquid density and an increase of the interfacial thickness and of the vapor density.

It is now very interesting to check if the shape of the density profiles can be fitted by using the same function as that used for the density profiles calculated from atomistic

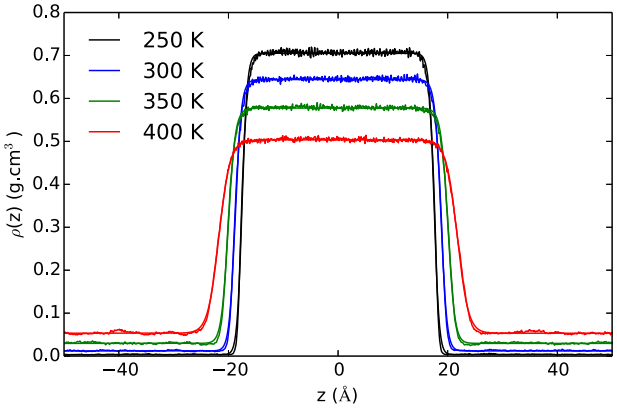

FIG. 4. Density profiles along the normal surface calculated in a simulation carried out with the multi-temperature CG potential U_{MT}^{C} at 250, 300, 350, and 400 K for *n*-pentane liquid-vapor phase equilibria. The smooth lines represent the fitted tangent hyperbolic function.

Reuse of AIP Publishing content is subject to the terms: https://publishing.aip.org/authors/rights-and-permissions. Downloaded to IP: 195.221.123.85 On: Wed, 17 Aug 2016 07:32:51

MC and MD simulations.[54,55] The resulting fitting curves are represented in Figure 4. The shape of the density profiles matches very well with that of the hyperbolic tangent function of the form

$$\rho(z) = \frac{1}{2}(\rho_l + \rho_v) - \frac{1}{2}(\rho_l - \rho_v)\tanh(\frac{2(z - z_0)}{\delta}), \quad (9)$$

where ρ_l and ρ_v are the liquid and vapor phases densities, respectively. z_0 indicates the position of the Gibbs dividing surface and δ represents the interfacial thickness.

We now focus on a quantitative comparison between the coexisting densities calculated from Eq. (9) and those calculated from atomistic simulations. The coexistence curves as a function of temperature for DPD and MD simulations are shown in Figure 5. It can be seen that the DPD curve with 300 K potential closely follows the MD reference curve between 250 K and 400 K, but moves away at higher temperature, with a critical point estimated around 570 K whereas the MD critical point is around 460 K and the experimental corresponding point is 470 K. The DPD curve with the multi-temperature potential is slightly less faithful to the MD curve, especially at low temperature with a deviation around 10% at 250 K. However, the critical point is much better reproduced, so that the multi-temperature potential performs better than the 300 K potential above 400 K. It is also noticeable that the accuracy of the DPD phase densities relative to MD simulations is comparable to the deviation between MD and experiments.

The surface tension of the pentane interface was computed using the expression

$$\gamma = \frac{1}{2} L_z \left(P_{zz} - \frac{1}{2}(P_{xx} + P_{yy}) \right), \quad (10)$$

where P_{zz}, P_{xx}, and P_{yy} are average components of the pressure tensor. We also check the mechanical equilibrium inside the simulation box by calculating the surface tension along the z-axis by using the following definition:[56–58]

$$\gamma(z) = \int_z^{L_z/2} \Big(P_{\mathrm{N}}(z) - P_{\mathrm{T}}(z) \Big) dz, \quad (11)$$

where P_{N} (z) and $P_{\mathrm{T}}(z)$ are the normal and tangential pressure tensor elements. A comprehensive description of the calculation of these local elements can be found in Ref. 45. The different profiles of the pressure components shown in Figure 6 are decomposed into the kinetic or ideal part $\rho(z)k_BT$ and the configurational parts P_N and P_T. The profiles of the configurational parts of P_N and P_T are constant and similar in the bulk region phases. The profile of the difference $P_N - P_T$ leads to a zero contribution in the liquid and vapor phases in agreement with the mechanical equilibrium of the planar liquid-vapor interface. The profile also shows one peak at the interface region due to the negative contribution of the tangential part P_T. The integration of this profile gives the local surface tension $\gamma(z)$ (see Figure 6). The analysis of this profile indicates that the two interfaces contribute in the same way to the surface tension and that the liquid region does not bring any contribution as expected for a well-equilibrated two-phase system. We now report the values of the surface tension calculated by using the DPD CG model with those obtained by atomistic MD simulations. The comparison between the surface tensions obtained from MD and DPD is shown in Figure 7. The agreement between DPD and MD simulations using the multi-temperature potential is excellent in the whole range of temperatures. It is similar to the agreement between MD and experiments. In the range from 200 K to 400 K, the deviations between the surface tensions calculated with the CG DPD model and experiments are less than 15%. On the other hand, the surface tensions from DPD simulations using the 300 K potential are 5–10 mN m^{-1} too high. This is consistent with the critical point being largely overestimated using this potential, because the surface tension has to vanish at the critical point where the interface disappears. At this point, it is important to underline that the development of a CG model capable to reproduce the surface tensions over a large

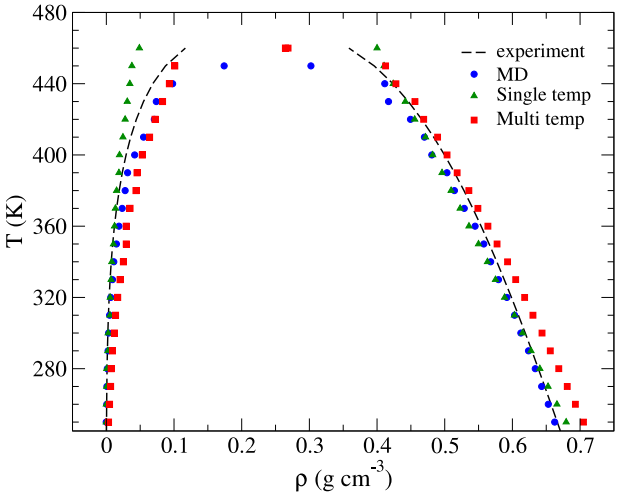

FIG. 5. Liquid-vapor coexistence density curves of *n*-pentane from experiments, molecular dynamics, DPD simulation with the potential $U^C_{300\mathrm{K}}$ optimized at 300 K, and DPD simulation with multi-temperature potential U^C_{MT}.

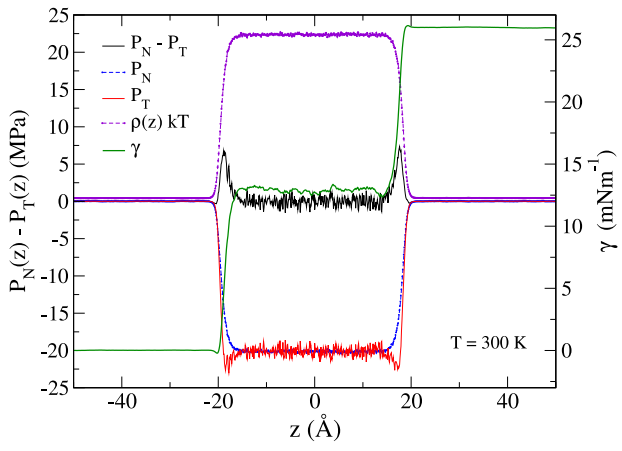

FIG. 6. Profile of the different contributions to the normal P_N and tangential P_T pressure components calculated at $T = 300$ K obtained from the multi-temperature potential U^C_{MT}. The difference $(P_N - P_T)$ is plotted and the profile integral $\gamma(z) = 1/2\int_{-L_z/2}^{z}(P_{\mathrm{N}}(z) - P_{\mathrm{T}}(z))\mathrm{d}z$ is represented in the right hand axis.

Reuse of AIP Publishing content is subject to the terms: https://publishing.aip.org/authors/rights-and-permissions. Downloaded to IP: 195.221.123.85 On: Wed, 17 Aug 2016 07:32:51

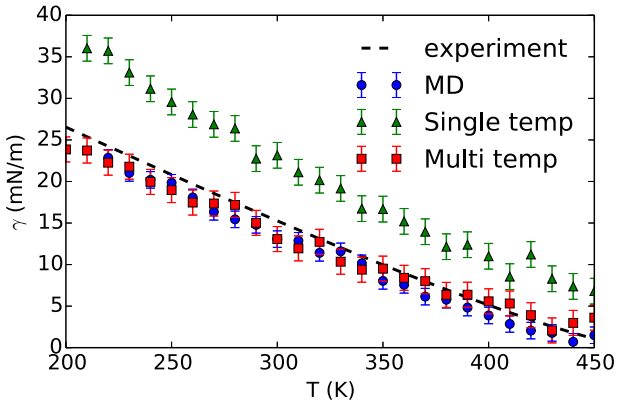

FIG. 7. Computed surface tension γ as a function of the temperature from experiments, molecular dynamics, DPD using the 300 K potential U^C_{300K}, and DPD using the multi-temperature potential U^C_{MT}.

range of temperatures is very interesting for more complex systems involving surfactants, for example. This preliminary study opens the way of using the methodology developed here for quantitative predictions of interfacial tensions of oil-water-surfactant systems of specific chemistry. Actually, the DPD models have already been applied to complex interfacial systems but by considering generic potential models not designed to molecules of specific chemistry.

The vapor pressure can be obtained from the pressure profile in the vapor phase. Since we did not have the MD pressure profile, we instead estimated the vapor pressure as the average P_{zz}. For MD simulations, we corrected the long range contribution of the Lennard-Jones tail to P_{zz} in order to account for the heterogeneity of density. This was done by rescaling the long-range correction from DLPOLY by a factor $(\frac{\rho_V}{\langle\rho\rangle})^2$. For DPD, no such correction is needed because the DPD potential is exactly zero beyond the cutoff. In Figure 8, the vapor pressure is plotted as a function of temperature. In the whole temperature range between 300 and 450 K, an excellent agreement is observed between MD and DPD using the multi-temperature potential, even better than that between MD and experiments. On the other hand, the vapor pressure from DPD using the 300 K potential is largely underestimated. This contrasts with the better agreement regarding density (Figure 5).

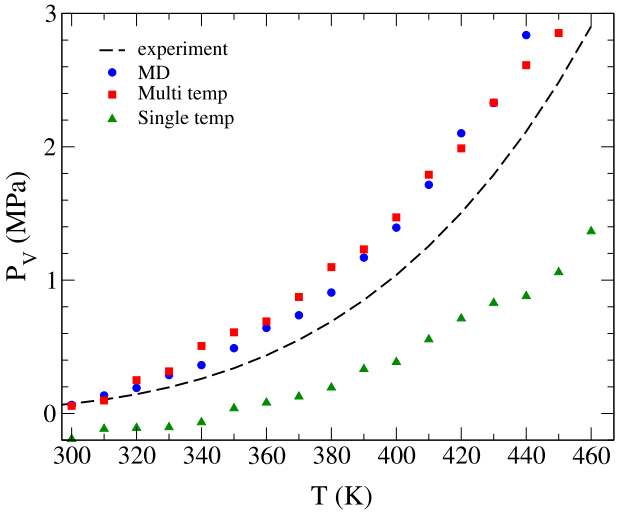

FIG. 8. Vapor pressure as a function of temperature from experiments, MD simulations, DPD simulations with the multi-temperature potential U^C_{MT}, and DPD simulations with the 300 K potential U^C_{300K}.

V. CONCLUSION

The simulation of coarse-grained models for the calculation of interfacial properties is an important area of active research. An important feature of the problem is to build a mesoscale model from an atomistic model. This is not straightforward because techniques such as iterative Boltzmann inversion or force-matching while applicable to homogeneous fluids are difficult to use in interfacial simulations because the effective potential may depend strongly on the local density. Here, we take the route of using the trajectory-based Bayesian method for the optimization of the CG model.

The trajectory-based Bayesian method for the optimization of DPD models[39] was extended to allow for using several reference trajectories at different temperatures. The transferability of the DPD potentials developed using this method was investigated. A single bead DPD model of *n*-pentane was optimized using reference MD trajectories at different temperatures in the constant-*NPT* ensemble. The bulk structure and density of the DPD model are in good agreement with the MD reference on a range of more than 150 K.

Then, the liquid-vapor interface was studied using the model optimized with bulk simulations. Far enough from the critical point, the density of the phases is very well reproduced using a single temperature potential (300 K). Below 400 K, the multi-temperature potential performs slightly less well regarding densities. The main advantage of the multi-temperature potential is that it gives good results up to the critical point. Using the multi-temperature potential, the surface tension and the vapor pressure of the DPD model are in excellent agreement with the MD model used as a reference. For these properties, the single-temperature potential stays in the background.

Globally, we have shown that it is possible to develop a DPD potential with a good transferability in temperature regarding bulk structures and interfacial properties. The DPD potentials have been developed in the *NPT* ensemble at a given pressure. We have not investigated the transferability to other pressures. In principle, several reference trajectories at different pressures can be used for the optimization. This could improve the compressibility and the P, ρ phase diagram of the DPD model and is a possible extension of this work.

In the future, the modeling of complex interfacial systems involving a significant number of molecules of each species and longer times to ensure equilibration of the species between the phases will require the use of CG models in mesoscopic simulations. The CG models must consider the chemical structure of the different species. The methodology reported here offers an opportunity to develop realistic CG potential models that could be applied to the calculation of interfacial tensions of complex systems.

Reuse of AIP Publishing content is subject to the terms: https://publishing.aip.org/authors/rights-and-permissions. Downloaded to IP: 195.221.123.85 On: Wed, 17 Aug 2016 07:32:51

ACKNOWLEDGMENTS

The authors thank the Région Auvergne for funding (*projet Nouveau Chercheur*).

[1]J. C. Shelley, M. Y. Shelley, R. C. Reeder, S. Bandyopadhyay, and M. L. Klein, J. Phys. Chem. B **105**, 4464 (2001).
[2]S. O. Nielsen, C. F. Lopez, G. Srinivas, and M. L. Klein, J. Phys.: Condens. Matter **16**, R481 (2004).
[3]M. L. Klein and W. Shinoda, Science **321**, 798 (2008).
[4]S. Riniker, J. R. Allisonab, and W. F. van Gunsteren, Phys. Chem. Chem. Phys. **14**, 12423 (2012).
[5]G. Maurel, B. Schnell, F. Goujon, M. Couty, and P. Malfreyt, J. Chem. Theory Comput. **8**, 4570 (2012).
[6]G. Maurel, F. Goujon, B. Schnell, and P. Malfreyt, RSC Adv. **5**, 14065 (2015).
[7]G. Maurel, F. Goujon, B. Schnell, and P. Malfreyt, J. Phys. Chem. C **119**, 4817 (2015).
[8]M. Ndao, J. Devemy, A. Ghoufi, and P. Malfreyt, J. Chem. Theory Comput. **11**, 3818 (2015).
[9]J. W. Chu, S. Izbeko, and G. A. Voth, Mol. Simul. **32**, 211 (2006).
[10]C. Peter and K. Kremer, Soft Matter **5**, 4357 (2009).
[11]G. A. Voth, *Coarse-Graining of Condensed Phase and Biomolecular Systems* (CRC Press, 2009).
[12]C. Peter and K. Kremer, Faraday Discuss. **144**, 9 (2010).
[13]Y. Li, B. C. Abberton, M. Kröger, and W. K. Liu, Polymers **5**, 751 (2013).
[14]S. O. Nielsen, C. F. Lopez, G. Srinivas, and M. L. Klein, J. Chem. Phys. **119**, 7043 (2003).
[15]W. Shinoda, R. DeVane, and M. L. Klein, Mol. Simul. **33**, 27 (2007).
[16]C. Avendaño, T. Lafitte, A. Galindo, C. S. Adjiman, G. Jackson, and E. A. Müller, J. Phys. Chem. B **115**, 11154 (2011).
[17]W. G. Noid, J.-W. Chu, G. S. Ayton, V. Krishna, S. Izvekov, G. A. Voth, A. Das, and H. C. Andersen, J. Chem. Phys. **128**, 244114 (2008).
[18]P. Español and I. Zúñiga, Phys. Chem. Chem. Phys. **13**, 10538 (2011).
[19]G. Deichmann, V. Marcon, and N. F. A. van der Vegt, J. Chem. Phys. **141**, 224109 (2014).
[20]S. Markutsya and M. H. Lamm, J. Chem. Phys. **141**, 174107 (2014).
[21]S. Trément, B. Schnell, L. Petitjean, M. Couty, and B. Rousseau, J. Chem. Phys. **140**, 134113 (2014).
[22]D. Reith, M. Pütz, and F. Müller-Plathe, J. Comput. Chem. **24**, 1624 (2003).
[23]A. P. Lyubartsev and A. Laaksonen, Phys. Rev. E **52**, 3730 (1995).
[24]S. Izvekov and G. A. Voth, J. Phys. Chem. B **109**, 2469 (2005).
[25]S. J. Marrink, A. H. de Vries, and A. E. Mark, J. Phys. Chem. B **108**, 750 (2004).
[26]S. J. Marrink, H. J. Risselada, S. Yefimov, D. P. Tieleman, and A. H. de Vries, J. Phys. Chem. B **111**, 7812 (2007).
[27]S. W. Chiu, H. L. Scott, and E. Jakobsson, J. Chem. Theory Comput. **6**, 851 (2010).
[28]R. DeVane, W. Shinoda, P. B. Moore, and M. L. Klein, J. Chem. Theory Comput. **5**, 2115 (2009).
[29]W. Chapman, K. Gubbins, G. Jackson, and M. Radosz, Fluid Phase Equilib. **52**, 31 (1989).
[30]W. Chapman, K. Gubbins, G. Jackson, and M. Radosz, Ind. Eng. Chem. Res. **29**, 1709 (1990).
[31]C. Avendano, T. Lafitte, A. Galindo, C. S. Adjiman, G. Jackson, and E. A. Müllerller, J. Phys. Chem. B **117**, 2717 (2013).
[32]F. Cao and H. Sun, J. Chem. Theory Comput. **11**, 4760 (2015).
[33]S. O. Yesylevskyy, L. V. Schäfer, D. Sengupta, and S. J. Marrink, PLoS Comput. Biol. **6**, 1 (2010).
[34]P. J. Hoogerbrugge and J. M. V. A. Koelman, Europhys. Lett. **19**, 155 (1992).
[35]R. D. Groot and P. B. Warren, J. Chem. Phys. **107**, 4423 (1997).
[36]P. B. Warren, Phys. Rev. E **68**, 066702 (2003).
[37]A. Ghoufi and P. Malfreyt, Phys. Rev. E **83**, 051601 (2011).
[38]P. Español and P. B. Warren, Europhys. Lett. **30**, 191 (1995).
[39]A. Dequidt and J. G. S. Canchaya, J. Chem. Phys. **143**, 084122 (2015).
[40]C. Hijón, M. Serrano, and P. Español, J. Chem. Phys. **125**, 204101 (2006).
[41]C. Hijón, P. Español, E. Vanden-Eijnden, and R. Delgado-Buscalioni, Faraday Discuss. **144**, 301 (2010).
[42]M. Arienti, W. Pan, X. Li, and G. Karniadakis, J. Chem. Phys. **134**, 204114 (2011).
[43]A. Ghoufi and P. Malfreyt, Eur. Phys. J. E **36**, 10 (2013).
[44]A. Ghoufi and P. Malfreyt, J. Chem. Theory Comput. **8**, 787 (2012).
[45]A. Ghoufi, P. Malfreyt, and D. J. Tildesley, Chem. Soc. Rev. **45**, 1387 (2016).
[46]T. P. Liyana-Arachchi, S. N. Jamadagni, D. Eike, P. H. Koenig, and J. I. Siepmann, J. Chem. Phys. **142**, 044902 (2015).
[47]E. Mayoral and A. G. Goicochea, J. Chem. Phys. **138**, 094703 (2013).
[48]I. T. Todorov, W. Smith, K. Trachenko, and M. T. Dove, J. Mater. Chem. **16**, 1911 (2006).
[49]M. G. Martin and J. I. Siepmann, J. Phys. Chem. B **102**, 2569 (1998).
[50]F. Goujon, P. Malfreyt, A. Boutin, and A. H. Fuchs, J. Chem. Phys. **116**, 8106 (2002).
[51]J.-C. Neyt, A. Wender, V. Lachet, A. Ghoufi, and P. Malfreyt, J. Chem. Theory Comput. **10**, 1887 (2014).
[52]H. J. C. Berendsen, J. P. M. Postma, W. F. van Gunsteren, A. DiNola, and J. R. Haak, J. Chem. Phys. **81**, 3684 (1984).
[53]R. Potestio, JUnQ **3**, 13 (2013).
[54]J. C. Neyt, A. Wender, V. Lachet, and P. Malfreyt, J. Phys. Chem. B **115**, 9421 (2011).
[55]F. Biscay, A. Ghoufi, and P. Malfreyt, J. Chem. Phys. **134**, 044709 (2011).
[56]J. G. Kirkwood and F. P. Buff, J. Chem. Phys. **17**, 338 (1949).
[57]J. H. Irving and J. Kirkwood, J. Chem. Phys. **18**, 817 (1950).
[58]J. S. Rowlinson and B. Widom, *Molecular Theory of Capillarity* (Clarendon Press, Oxford, 1982).

Reuse of AIP Publishing content is subject to the terms: https://publishing.aip.org/authors/rights-and-permissions. Downloaded to IP: 195.221.123.85 On: Wed, 17 Aug 2016 07:32:51